Solar Energy Materials & Solar Cells 208 (2020) 110395

Contents lists available at ScienceDirect

Solar Energy Materials and Solar Cells

journal homepage: http://www.elsevier.com/locate/solmat

Realizing efficient natural sunlight-driven photothermal selective catalytic reduction of nitrogen oxides by AlN_x assisted W doped Fe_2O_3 nanosheets

Xianhua Bai [a,1], Dachao Yuan [b,1], Yingqi Xu [a], Yaguang Li [a,*], Wen Lu [c], Shufang Wang [a], Guangsheng Fu [a], Yong Hu [c,**]

[a] Hebei Key Lab of Optic-electronic Information and Materials, The College of Physics Science and Technology, Hebei University, Baoding, 071002, China
[b] College of Mechanical and Electrical Engineering, Hebei Agricultural University, Baoding, 071001, China
[c] Department of Chemistry, Zhejiang Normal University, Jinhua, Zhejiang, 321004, China

ARTICLE INFO

Keywords:
AlN_x
Fe_2O_3
Photocatalysis
Photothermal
NO_x SCR

ABSTRACT

Photocatalytic selective catalytic reduction of nitrogen oxides (NO_x SCR) is a green and effective method to eliminate NO_x. But the natural sunlight-driven NO_x SCR is not realized due to the low temperature under sparse sunlight irradiation and the lack of highly active catalysts. To solve those problems, we selected a commercial AlN_x film which can heat the catalysts to 270 °C just under one standard solar irradiation because of its full sunlight absorption and low radiation characteristics, enabling to onset NO_x SCR. Further, a polyvinyl alcohol assisted graphene oxides templated method was developed to synthesize the W doped Fe_2O_3 nanosheets on a large scale, which can be used as efficient NO_x SCR catalysts with high N_2 selectivity, excellent SO_2 and H_2O resistances. As a result, the AlN_x assisted W doped Fe_2O_3 nanosheets showed 92% and 90% NO conversion rate under one solar irradiation and outdoor sunlight irradiation respectively without second energy input, first time of realizing natural sunlight-driven photothermal NO_x SCR. This strategy demonstrates a great potential on second energy free industrialized NO_x SCR.

1. Introduction

Nitrogen oxides (NO_x) are one of the most poisonous gases that lead to tremendous environmental problems [1], such as photochemical smog and acid rain [2]. A number of strategies have been developed to eliminate NO_x ($deNO_x$) [3–5]. Amongst, selective catalytic reduction of NO_x by ammonia (NO_x SCR) is the main $deNO_x$ technology due to its green emission, low cost and excellent oxygen tolerance [6]. However, industrial NO_x SCR is commonly operated at least 200 °C temperature [7], which requires huge amount of thermal power and expensive equipment, causing enormous waste of second energy and capital [8,9]. Constructing efficient second energy free NO_x SCR system is of great significance for human society. Sunlight-driven catalysis can convert the photons as energy [10,11]. By far, the reports on photocatalytic $deNO_x$ are photocatalytic oxidation, which introduce secondary pollution eg., NO_2, NO_3, not suitable for practical application [12,13]. Besides photocatalytic oxidation, photothermal catalysis has been reported for sunlight-driven NO_x SCR [14,15]. However, those photothermal catalysts require second energy input and light irradiation simultaneously to drive NO_x SCR [16,17], making the current photothermal NO_x SCR useless [18]. To date, employing a weak sunlight source (1 kW m^{-2} level) to operate photothermal NO_x SCR without second energy input is still a challenge [18,19].

On the other hand, multiple metal oxides such as MnO_2(Ce)/TiO_2 [20–22], $Ce_aTa_bO_x$ [23] and Cu-zeolites [24–26] have been developed as the NO_x SCR catalysts with SO_2 and H_2O resistances [27,28]. But the activities of those multiple metal oxides can still not meet the requirements [29,30]. Two dimensional (2D) materials have the merits of high surface area and exotic electronic properties [17,31,32]. Therefore, the preparation of NO_x SCR catalysts as nanosheets can further improve the NO_x SCR efficiency of multiple metal oxides.

Herein, taking W doped Fe_2O_3 (an excellent anti-toxic NO_x SCR catalyst) as an example, we developed a graphene oxides templated method, which can large scale produce W doped Fe_2O_3 nanosheets in the

* Corresponding author.
** Corresponding author.
E-mail addresses: yaguang_1987@126.com (Y. Li), yonghu@zjnu.edu.cn (Y. Hu).
[1] These authors contributed equally to this work.

https://doi.org/10.1016/j.solmat.2020.110395
Received 19 October 2019; Received in revised form 6 December 2019; Accepted 7 January 2020
Available online 16 January 2020

presence of polyvinyl alcohol. Compared with the bulk W doped Fe_2O_3, W doped Fe_2O_3 nanosheets showed more wide operation temperature window, higher NO_x SCR activity and excellent SO_2, H_2O resistances. Furthermore, we used a commercial AlN_x film to construct the NO_x SCR reactor, which can heat the W doped Fe_2O_3 nanosheets to more than 270 °C high temperature under standard solar light irradiation due to the full sunlight absorption and low radiation of AlN_x film. Therefore, the AlN_x film assisted W doped Fe_2O_3 nanosheets can realize an efficient second energy free natural sunlight-driven photothermal NO_x SCR.

2. Experimental Section

Chemicals: Ferric nitrate ($Fe(NO_3)_3$ $9H_2O$) and ammonium metatungstate ($H_{28}N_6O_{41}W_{12}$) were purchased from Sinopharm Co., Ltd. Polyvinyl alcohol (PVA 224) was purchased from Aladdin Co., Ltd. Liquid nitrogen was purchased from Baoding Xicheng special gas Co., Ltd. The AlN_x film was provided by Tsinghua Solar Co., Ltd. All chemicals were directly used as received without further treatment.

Synthesis of W doped Fe_2O_3 nanosheets: To synthesize W doped Fe_2O_3 (W/Fe_2O_3) nanosheets, we selected the graphene oxide (GO) sheet as the substrates. Firstly, 6.07 g of $Fe(NO_3)_3$ $9H_2O$ and 0.15 g of $H_{28}N_6O_{41}W_1$ were dispersed in 20 ml of water (named as A solution); 1000 mg of PVA 224 was dissolved in 10 ml of water by heating and then added the PVA solution into 500 ml of GO aqueous solution (2 mg/ml) to mixed as B solution. Secondly, A solution was dropped into B solution within 1 h. Subsequently, the mixed solution was frozen by liquid nitrogen as an ice cube and freeze-dried for 1 week to remove water. The dried product was calcined in the air with 500 °C for 12 h to remove the GO nanosheets and PVA as well as mineralize the metal ions as 2D metal oxide nanosheets.

Synthesis of bulk W/Fe_2O_3: The process of synthesizing bulk W doped Fe_2O_3 was similar to that of preparing W doped Fe_2O_3 nanosheets without adding PVA 224 in GO solution.

The W/W + Fe atomic ratio in the two samples is 0.04.

Characterizations: We used the scanning electron microscopy (SEM, FEI Nova Nano SEM450), transmission electron microscopy (TEM, JEOL 2100F) to identify the morphology, crystal structure of samples. Energy Dispersive X-Ray Spectroscopy (EDS) mapping and selected area electron diffraction (SAED) were detected by JEOL 2100F. The phase was detected by the powder X-ray diffraction (XRD) operated at 20 kV and 30 mA with Cu Kα radiation (λ = 1.5406 Å). The X-ray photoelectron spectroscopic (XPS) spectra were detected by Thermo ESCALAB-250 spectrometer with a monochromatic Al Kα radiation source (1486.6 eV). The binding energies determined by XPS were corrected with reference of adventitious carbon peak (284.6 eV) for each sample. The Brunauer–Emmett–Teller (BET) surface area was measured by Micromeritics Tristar 3030 system. Platinum resistance thermometer (M363886) was used to detect the temperature of all materials. The light absorption property of W/Fe_2O_3 nanosheets and AlN_x was detected by a Shimadzu UV3600 UV–vis spectrophotometer.

Thermal SCR test: The steady state NH_3-SCR NO_x reaction activity was tested in a fixed-bed quartz tube reactor containing 0.6 ml of catalysts (0.1 g of 4% W/Fe_2O_3 nanosheets or 0.7 g of bulk W/Fe_2O_3, to make the same volume of catalysts), and the reaction conditions were controlled as follows: 1000 ppm NO, 1000 ppm NH_3, 5 vol% O_2, 100 ppm SO_2 (when used), 3% H_2O (when used) and N_2 balance; 200 ml/min (sccm) total flow rate and the gas hourly space velocity (GHSV) was 20,000 h^{-1}. Water vapor was generated by passing N_2 through a heated gas-wash bottle containing de-ionized water. The effluent gas, including NO, NO_2, NH_3 and N_2O was analyzed by a FTIR spectrometer (Gasmet FTIR DX4000) [21,33]. The traditional photothermal SCR test was the cooperation of thermal and photothermal energy. Therefore, it was still operated in this system and a xenon lamp (Microsolar 300) was used as the light source to irradiate the catalysts while heating the catalysts. The UV–vis optical property of materials was investigated on a Shimadzu UV3600 UV–vis spectrophotometer.

Calculation of thermal radiation: The calculation of thermal radiation was according to the Stefan–Boltzmann law:

$$J = \varepsilon\sigma\left(T_1^4 - T_2^4\right)$$

J is the thermal radiation energy, σ is the constant, ε is the emissivity of materials, T_1 and T_2 are the 543 K (270 °C) and 308 K (35 °C) respectively. The ε of W/Fe_2O_3 nanosheets and AlN_x film was 0.97 and 0.1 at 270 °C respectively, which were provided by Hangzhou Ruijia Precision Science Instrument Co., Ltd. According to the ε of W/Fe_2O_3 nanosheets and AlN_x film at 270 °C, the simulated thermal radiation of W/Fe_2O_3 nanosheets and AlN_x film was 4.68 and 0.50 kW m^{-2}, respectively.

Sunlight-driven AlN_x assisted SCR test: The AlN_x film was coated on the outside of flow-type tube and then covered with a vacuum layer ($1.3*10^{-3}$ Pa pressure) as shown in Fig. S1. 0.6 ml of catalysts (0.1 g of 4% W/Fe_2O_3 nanosheets or 0.7 g of bulk W/Fe_2O_3, to make the same volume of catalysts) were dispersed by 10 ml of ethanol and then loaded in the inner of the flow-type tube, drying by the irradiation of outdoor sunlight (Fig. S2). The feeding gas controlled as follows: 1000 ppm NO, 1000 ppm NH_3, 5 vol% O_2, 100 ppm SO_2 (when used), 3% H_2O (when used) and N_2 balance, 200 sccm total flow rate. The gas hourly space velocity (GHSV) was 20,000 h^{-1}.

Natural sunlight-driven AlN_x assisted SCR test: The natural test was similar to that of photothermal catalysis test. The differences are the following: 1. Outdoor sunlight was the light source. 2. A parabolic reflector (Fig. S3) with 4 times concentration was used to concentrate solar light.

3. Results and discussions

W doped Fe_2O_3 (W/Fe_2O_3) is a typical NO_x SCR catalyst with excellent H_2O and SO_2 tolerance [34]. Taking W/Fe_2O_3 as an example, we showed a gram scale production of W/Fe_2O_3 nanosheets by the modified GO templated method. As illustrated in Fig. 1a, we firstly added PVA into the GO solution to make it have high viscosity. Then, massive W and Fe precursors were added in the high viscosity solution. Subsequently, the water was removed by freeze-drying process. The dried product was annealed in the air with 500 °C to form the W/Fe_2O_3 nanosheets (W/W + Fe ratio is 4%, unless stated) while oxidizing the GO and PVA as CO_2 by oxygen. Raman spectrum (Fig. 1b) of this sample exhibited four characteristic peaks of hematite at 220, 281, 403, and 602 cm^{-1} [35], confirming the Fe_2O_3 phase. But, the two peaks at ~238 and 491 cm^{-1} [36], which are visible in crystalline Fe_2O_3, were missed from W/Fe_2O_3 nanosheets, showing low crystallinity of this sample. XRD showed no peaks of W/Fe_2O_3 nanosheets, indicating a probably amorphous state of materials (Fig. 1c). SEM image showed the curved nanosheets morphology of the obtained sample (Fig. 1d). To make a comparison, we also applied the GO templated method to synthesize W/Fe_2O_3 without adding PVA. In the absence of PVA, the metal ions could cause the agglomeration of GO in solution, resulting in more than 100 nm thick sheets and low surface area of 21 m^2 g^{-1} (bulk W/Fe_2O_3, Fig. S4). It has been reported that the excessive metal ions adsorbed on GO sheets could neutralize the electronegativity and introduce the layered stacking of GO, leading to the formation of thick metal oxides sheets [37]. PVA solution has high viscosity, which can delay the stacking of GO in the solution with excessive metal ions, so that the GO sheets were still separated after adsorbing massive metal precursors as shown in Fig. S5. The BET surface area of W/Fe_2O_3 nanosheets was 310 m^2 g^{-1} (Fig. S6a), conducive to achieve high catalytic activity. Therefore, the PVA assisted GO templated method can large-scale synthesize two-dimensional materials. TEM image depicts that the W/Fe_2O_3 nanosheets have a wrinkled surface (Fig. 1e). Elemental mapping images of Fe, W and O elements on W/Fe_2O_3 nanosheets reveal an even distribution over the whole region of nanosheets, indicting no phase separation (Fig. 1f). Further, the clear lattice fringes of W/Fe_2O_3 nanosheets were not observed in the High-resolution (HR) TEM image (Fig. 1g),

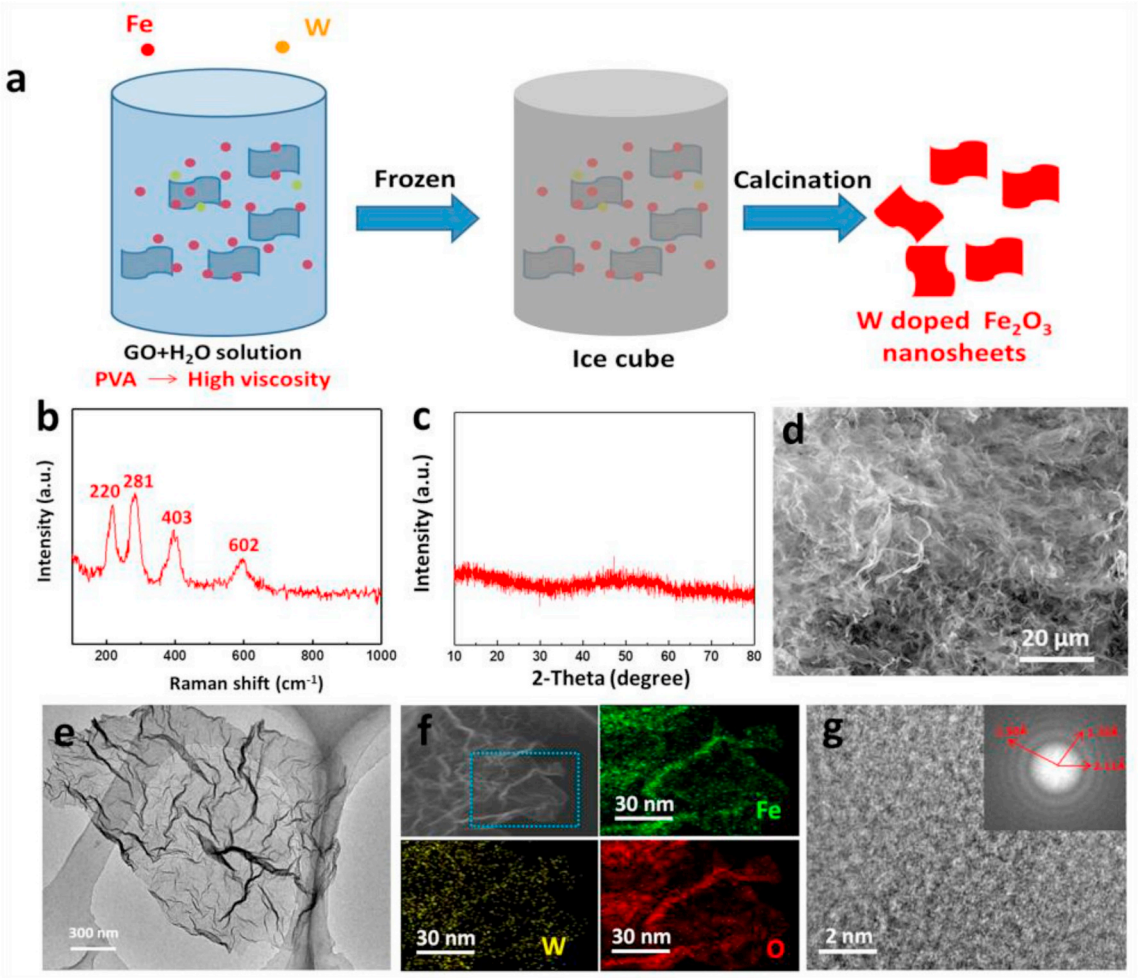

Fig. 1. (a) Schematic preparation of W doped Fe_2O_3 (W/Fe_2O_3) nanosheets. (b) Raman spectrum, (c) XRD pattern, (d) SEM image, (e) TEM image, (f) STEM image and EDS mapping images of Fe, W, O element for W doped Fe_2O_3 nanosheets. (g) High-resolution TEM image of W doped Fe_2O_3 nanosheets. Inset panel in Fig. 1g is the electron diffraction pattern.

evidencing its amorphous state. There are a few wide rings in the SAED pattern showed in Fig. 1g and the corresponding crystal distance was 2.11, 1.70 and 1.51 Å, respectively, which was similar to the (100), (004) and (103) planes of graphite [38]. We thought the widen diffraction rings might be originated from the carbon film on grid. Meanwhile, XPS revealed that the valence states of W and Fe in W/Fe_2O_3 nanosheets were +6 and + 3, respectively (Figs. S6b, c, d).

The thermal NO_x SCR performances of W/Fe_2O_3 nanosheets were tested at 200 sccm flux of feeding gas, in comparison with bulk W/Fe_2O_3. NO was used as NO_x source for SCR. In Fig. 2a, bulk W/Fe_2O_3 performed 3.1% NO conversion efficiency at 250 °C. Whereas, W/Fe_2O_3 nanosheets showed a 150 °C onset temperature for NO conversion and reached to 88% denitrification ($deNO_x$) efficiency at 250 °C, 28.3 times higher than that of bulk W/Fe_2O_3 (3.1%), indicating the nano-effect on increasing the NO_x SCR activity of W/Fe_2O_3 [39]. Not only excellent NO_x SCR activity, but W/Fe_2O_3 nanosheets also showed a 96% N_2 selectivity efficiency in all range of reaction temperature window (Fig. 2b). In order to apply on commercial NO_x SCR, H_2O and SO_2 were added in feeding gas respectively. Clearly, the $deNO_x$ rates through W/Fe_2O_3 nanosheets were retained in the presence of SO_2 (100 ppm) at 300 °C temperature, revealing robust resistance (Fig. 2c). Further, after adding 3% H_2O in feeding gas, the $deNO_x$ efficiency was a little lower than that using dry gases when the temperature was lower than 200 °C and it was identical to that using dry gases when the temperature was higher than 200 °C (Fig. 2d). Therefore, W/Fe_2O_3 nanosheets showed excellent $deNO_x$ performance in the presence of sulfurous gases and water vapor.

Despite the availability of highly active and stable W/Fe_2O_3 nanosheets, the NO_x SCR was not worked under standard one sunlight (1.0 kW m^{-2} intensity) irradiation (Fig. 3a). As shown in Fig. 3b, the one solar-driven NO_x SCR can be worked by using second energy to heat the W/Fe_2O_3 nanosheets to more than 150 °C. And the one solar-driven NO_x SCR efficiency was 23 and 67% when the W/Fe_2O_3 nanosheets heated to 150 and 200 °C respectively, higher than that of thermal NO_x SCR at corresponding temperatures (9 and 41% at 150 and 200 °C). Therefore, the photothermal catalysis is an auxiliary means to promote the efficiency of thermal NO_x SCR and cannot run the NO_x SCR independently under 1 solar irradiation, which is common in photothermal NO_x SCR. But, we still search the possibility of realizing weak sunlight-driven NO_x SCR. For W/Fe_2O_3 nanosheets, the sunlight absorption is not excellent. Fig. S7 showed that the W/Fe_2O_3 nanosheets only exhibited the photoresponse from 300 nm to 640 nm, less than 35% of sunlight region. Meanwhile, W/Fe_2O_3 nanosheets are blackbody-like materials with high emissivity, possessing violent heat radiation [12,13]. Assuming the temperature of W/Fe_2O_3 nanosheets located at 270 °C, the IR radiative heat loss can be as high as 4.68 kW m^{-2}, equivalent to 4.68 standard suns (based on Stefan-Boltzmann law, see details in Experimental Section), far exceeding the standard solar flux of 1 kW m^{-2}. Thus, the low

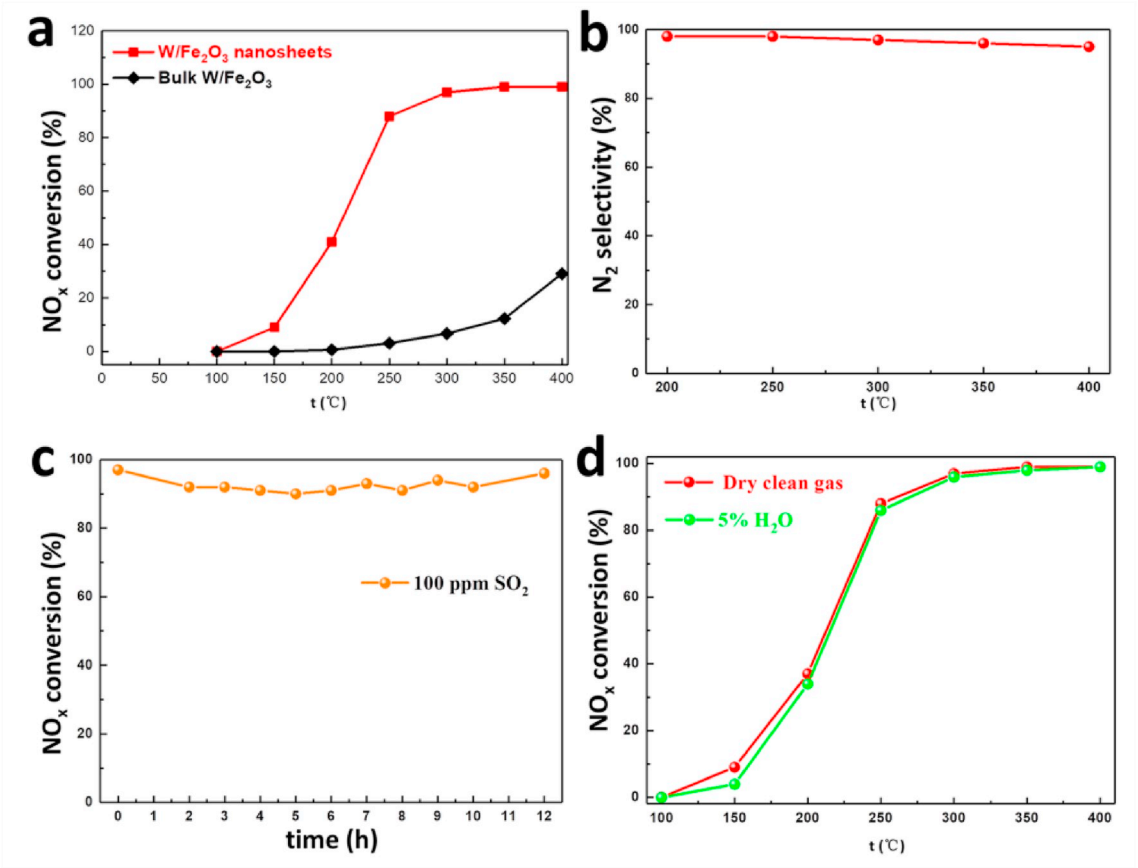

Fig. 2. (a) The NO_x SCR conversion performance over different catalysts under dry clean gas at gas hourly space velocity (GHSV) of 20,000 h^{-1}. (b) The corresponding N_2 selectivity along with reaction temperature over W/Fe_2O_3 nanosheets. (c) The NO_x conversion efficiency over W/Fe_2O_3 nanosheets under dry clean gas with 100 ppm SO_2 at 300 °C temperature and gas hourly space velocity (GHSV) of 20,000 h^{-1}. (d) The NO_x conversion efficiency over W/Fe_2O_3 nanosheets under dry clean gas with 3% H_2O at gas hourly space velocity (GHSV) of 20,000 h^{-1}. Dry clean gas is composed of 1000 ppm NO, 1000 ppm NH_3, 5 vol% O_2 and N_2 balance.

sunlight absorption and high IR radiation make the temperature of W/Fe_2O_3 nanosheets is far from meeting the requirements of NO_x SCR. In commercial solar water heaters, the light absorber was AlN_x film [40], which can heat the water reach to 100 °C just under outdoor sunlight irradiation due to the full sunlight absorption and little radiation. Therefore, we thought that the AlN_x film might be able to obtain enough high temperature for NO_x SCR. We used the commercial AlN_x film from Huangming solar water heater as the sunlight absorber (inset in Fig. 3c). As shown in Fig. 3c, SEM image shows that the AlN_x film has a thickness of 1 μm. XRD pattern confirmed that the film was composed of cubic AlN_x (PDF#25–1495, Fig. 3d). UV–Vis absorption spectrum of the AlN_x film exhibited obvious absorption from 300 nm to 1000 nm (Fig. 3e), accounting for nearly 100% of solar spectrum. Especially, different from the black-body materials, AlN_x film is the approximately infrared emitted free materials. According to simulated calculation, the radiative heat loss of selective light absorber was only 0.50 kW m^{-2} at 270 °C (see calculation details in Experimental Section), which is equal to 11% thermal radiation of W/Fe_2O_3 nanosheets and 50% of the standard solar flux. Therefore, the temperature of the vacuum layer protected AlN_x film was as high as 296 °C under 1 kW m^{-2} of sunlight irradiation [41]. Such a high temperature is enough to maintain the operation of NOx SCR. Therefore, we designed a photothermal system by AlN_x film and vacuum layer to full absorb sunlight and reduce the heat energy dissipation (Figs. S1 and 2). As shown in Fig. 3f, the sunlight absorption is achieved by AlN_x film instead of W/Fe_2O_3 nanosheets, guaranteeing full sunlight absorption as well as low heat energy radiation. The W/Fe_2O_3 nanosheets were cast on the AlN_x film, which maintained the absorbed energy efficient transferred from AlN_x film to the W/Fe_2O_3 nanosheets.

As shown in Fig. 4a, under one standard solar (1.0 kW m^{-2} intensity) irradiation, the temperature of W/Fe_2O_3 nanosheets was 276 °C with the assistance of AlN_x film, in comparison with the 79 °C of W/Fe_2O_3 nanosheets direct irradiated by the same light. Consequently, when the light intensity was higher than 0.6 kW m^{-2}, NO started to be converted through W/Fe_2O_3 nanosheets assisted by the selective light absorber, which had no second energy input (Fig. 4b). And the deNO_x efficiency can be reached to 92% under 1 solar irradiation (1 kW m^{-2}). It is the first time to realize weak sunlight-driven NO_x SCR. This result reveals the significant advantage of AlN_x film in weak sunlight-driven catalysis. Meanwhile, the N_2 selectivity through W/Fe_2O_3 nanosheets equipped with AlN_x film was higher than 96% during one solar irradiation for 12 h (Fig. 4c). It shows that the AlN_x film does not affect the high N_2 selectivity of W/Fe_2O_3 nanosheets. Further, the deNO_x performances were not clearly changed yet in the presence of H_2O and SO_2 in feeding gas during 12 h one sunlight irradiation (Fig. 4d).

Based on the above sunlight-driven catalytic data, we directly carried out the outdoor solar-driven test. The W/Fe_2O_3 nanosheets equipped with AlN_x film were placed at Hebei University and the experiment was carried out from 07:00 to 18:00 under natural sunlight irradiation without any other second energies input (Fig. 5a). As shown in Fig. 5b, NO was started to be converted at 10:00 a.m. and the converted efficiency was increased with time went on. The deNO_x efficiency was reached to a maximum 60% at 12:00. Since the outdoor sunlight is significantly lower than 1 kW m^{-2} intensity, a parabolic reflector with 4 times focusing (Fig. S3) was used to concentrate the sunlight. With the

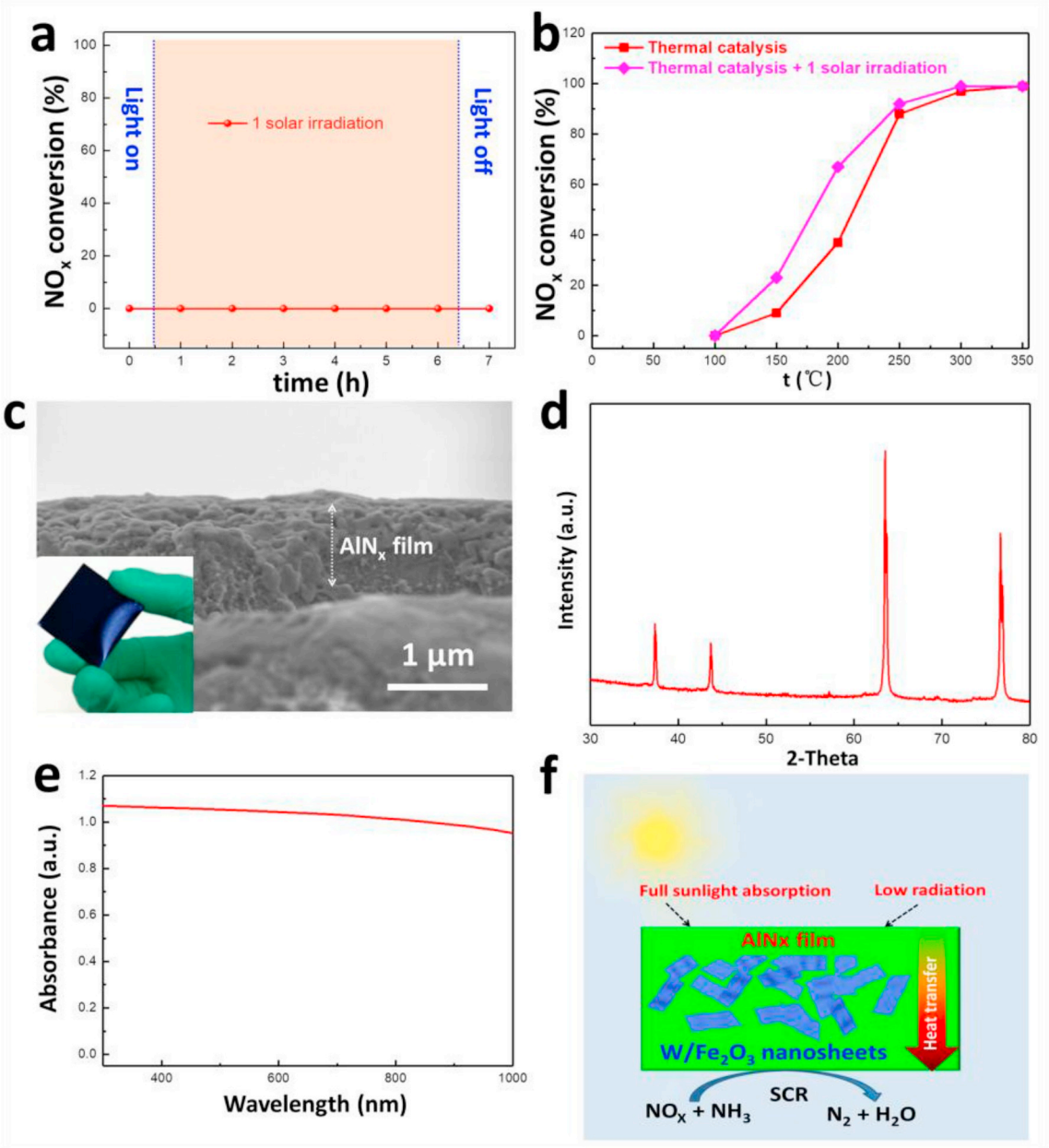

Fig. 3. (a) The direct 1 kW m^{-2} intensity of sunlight-driven NO_x SCR performance of W/Fe_2O_3 nanosheets without second energy input. (b) The thermal NO_x SCR performance of W/Fe_2O_3 nanosheets with (purple) and without (red) 1 kW m^{-2} intensity of sunlight irradiation. Dry clean gas at gas hourly space velocity (GHSV) of 20,000 h^{-1} (c) SEM, (d) XRD pattern, (e) normalized UV–Vis absorption spectrum of AlN_x film. The inset in Fig. 3c is the photograph of AlN_x film. (f) Schematic exhibition of solar-driven NO_x SCR through W/Fe_2O_3 nanosheets equipped with AlN_x film. (For interpretation of the references to colour in this figure legend, the reader is referred to the Web version of this article.)

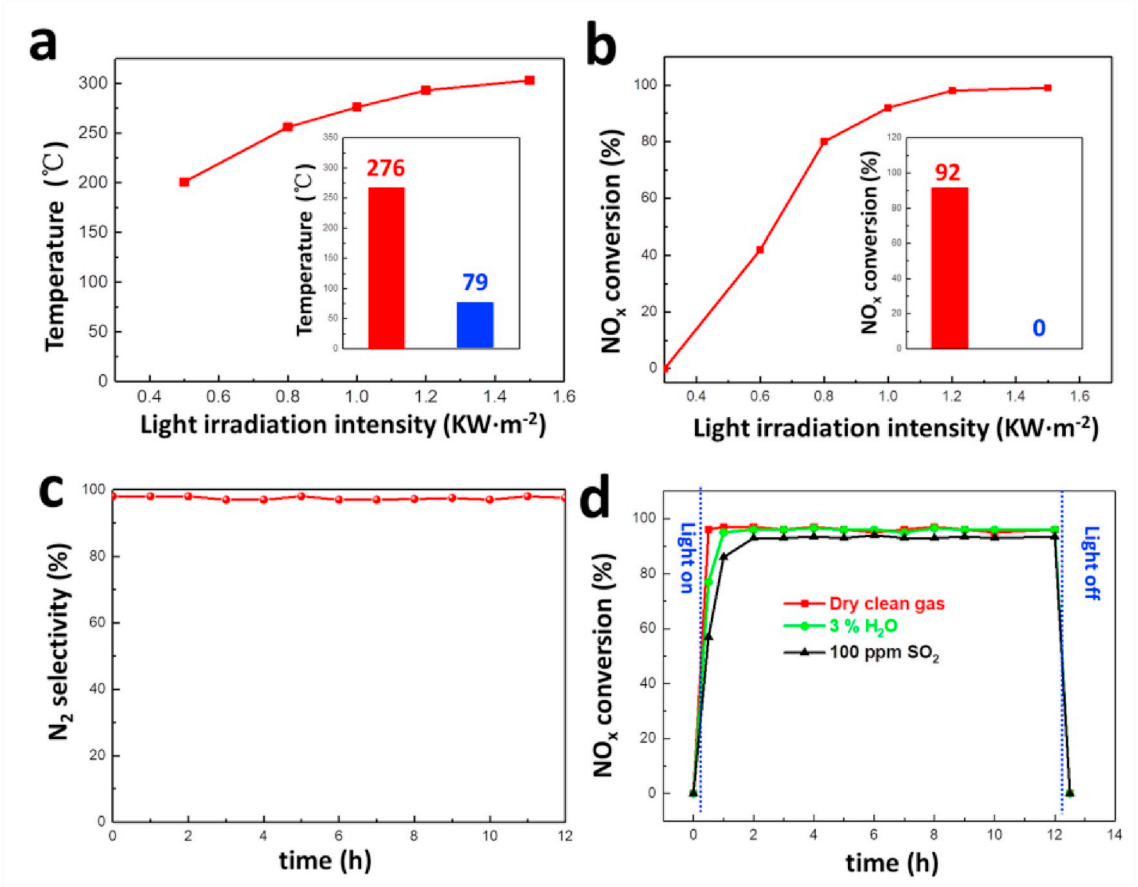

Fig. 4. (a) The light-driven temperature of W/Fe_2O_3 nanosheets equipped with AlN_x film, under direct light irradiation ranging from 0.5 to 1.5 kW m^{-2} intensity. The inset in Fig. 4a is the temperature of W/Fe_2O_3 nanosheets equipped with AlN_x film (red bar) and without AlN_x film (blue bar) irradiated by 1 kW m^{-2} intensity of sunlight. (b) is the corresponding light-driven NO_x conversion rates of W/Fe_2O_3 nanosheets equipped with AlN_x film. The inset in Fig. 4b is the NO_x conversion rates of W/Fe_2O_3 nanosheets equipped with AlN_x film (red bar) and without AlN_x film (blue bar) irradiated by 1 kW m^{-2} intensity of sunlight. The gas is the dry clean gas at gas hourly space velocity (GHSV) of 20,000 h^{-1}. (c) The N_2 selectivity of W/Fe_2O_3 nanosheets equipped with AlN_x film under the irradiation of 1 sun (1 kW m^{-2}) for 12 h. (d) The NO_x conversion efficiency over W/Fe_2O_3 nanosheets equipped with AlN_x film as a function of reaction time under dry clean gas with 100 ppm SO_2 and 3% H_2O under the irradiation of 1 sun (1 kW m^{-2}) for 12 h at gas hourly space velocity (GHSV) of 20,000 h^{-1}. Dry clean gas is composed of 1000 ppm NO, 1000 ppm NH_3, 5 vol% O_2 and N_2 balance. (For interpretation of the references to colour in this figure legend, the reader is referred to the Web version of this article.)

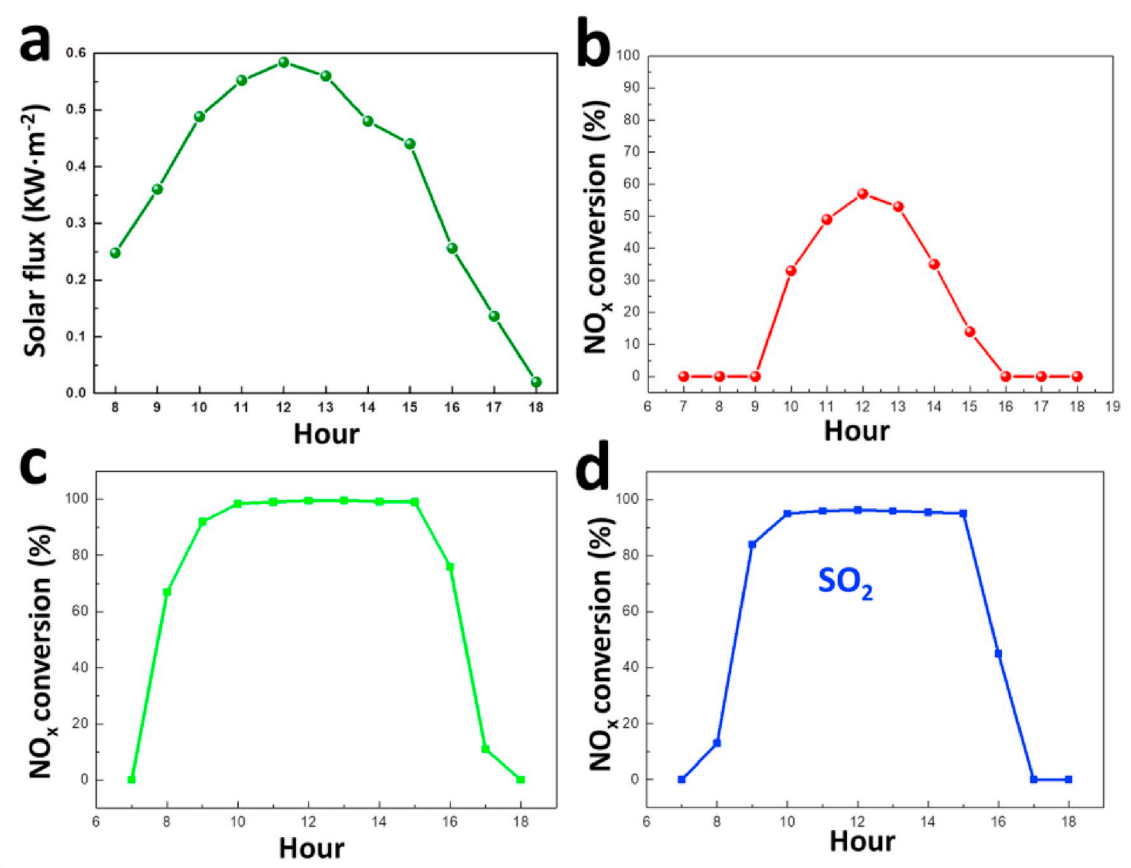

Fig. 5. (a) The solar flux on September 4, 2018, in Baoding, China. (b) The NO_x conversion of W/Fe_2O_3 nanosheets equipped with AlN_x film as a function of time under outdoor irradiation with the feeding gas under GHSV of 20,000 h^{-1}. Date: September 4, 2018, in Baoding, China. (c) The NO_x conversion of W/Fe_2O_3 nanosheets equipped with AlN_x film and a parabolic reflector as a function of time under outdoor irradiation with the feeding gas under GHSV of 20,000 h^{-1}. Date: September 23, 2018, in Baoding, China. (d) The NO_x conversion of W/Fe_2O_3 nanosheets equipped with AlN_x film and a parabolic reflector as a function of time under outdoor irradiation with the feeding gas (dry clean gas + 100 ppm SO_2) under GHSV of 20,000 h^{-1}. Date: September 24, 2018, in Baoding, China. Dry clean gas is composed of 1000 ppm NO, 1000 ppm NH_3, 5 vol% O_2 and N_2 balance.

assistance of focusing device, as shown in Fig. 5c, NO was started to convert at 8:00 a.m. and the $deNO_x$ efficiency was kept at more than 90% from 9:00 to 15:00 with dry gas. After adding SO_2 into reaction gas, the $deNO_x$ was still maintained at 90% level from 10:00 to 15:00 (Fig. 5d). Thus, the industrial grade NO_x SCR reaction could be carried out under outdoor sunlight irradiation.

4. Conclusions

In summary, we used PVA to prevent the stacking of GO to mass production of W doped Fe_2O_3 nanosheets at gram-scale. Due to the nanosheets morphology and high surface area of 310 m^2 g^{-1}, the as-synthesized W doped Fe_2O_3 nanosheets showed 96% N_2 selectivity, robust resistances for H_2O (3%) and SO_2 (100 ppm), 88% NO_x SCR efficiency at 250 °C, in comparison with the 3.1% rate of bulk W doped Fe_2O_3. Furthermore, the AlN_x film was applied to absorb sunlight, which could heat W doped Fe_2O_3 nanosheets to 276 °C only under 1 solar irradiation (AM 1.5G, 1 kW m^{-2}). As a result, the NO_x SCR reaction can achieve 92% $deNO_x$ efficiency through W doped Fe_2O_3 nanosheets equipped with AlN_x film under 1 solar irradiation and maintain more than 90% $deNO_x$ efficiency ranging from 10:00 to 16:00 under outdoor sunlight irradiation with the assistance of 4 times focusing parabolic reflector.

Author contributions

Y. G. Li and Y. Hu conceived the project and contributed to the design of the experiments and analysis of the data. X. H. Bai and D. C. Yuan performed the AlN_X assisted photothermal system preparation, characterizations. Y. Q. Xu and W. Lu performed the catalyst preparation, characterizations. X. H. Bai, D. C. Yuan, S. F. Wang, G. S. Fu wrote the paper. All the authors discussed the results and commented on the manuscript.

Declaration of competing interest

The authors declare that the research was conducted in the absence of any commercial or financial relationships that could be construed as a potential conflict of interest.

Acknowledgements

This work is supported by the National Natural Science Foundation of China of China (Grant No. 51702078), Hebei Provincial Department of Education Foundation (Grant No. BJ2019016) and Outstanding Doctoral Cultivation Project of Hebei University (YB201502). Thanks for the TEM technical supports provided by the Microanalysis Center, College of Physics Science and Technology, Hebei University.

Appendix A. Supplementary data

Supplementary data to this article can be found online at https://doi.org/10.1016/j.solmat.2020.110395.

References

[1] M. Radojevic, Environ. Pollut. 102 (1998) 685–689.
[2] J. Wang, H. Zhao, G. Haller, Y. Li, Appl. Catal. B Environ. 202 (2017) 346–354.
[3] J. Wang, H. Chen, Z. Hu, M. Yao, Y. Li, Catal. Rev. 57 (2014) 79–144.
[4] V. Alcalde-Santiago, A. Davó-Quiñonero, I. Such-Basáñez, D. Lozano-Castelló, A. Bueno-López, Appl. Catal. B Environ. 220 (2018) 524–532.
[5] S. Andonova, V. Marchionni, L. Lietti, L. Olsson, Mol. Catal. 436 (2017) 43–52.
[6] P.G. Smirniotis, et al., Angew. Chem. Int. Ed. 40 (2001) 2479–2482.
[7] Z. Yi, J. Ye, N. Kikugawa, T. Kako, S. Ouyang, H. Stuart-Williams, H. Yang, J. Cao, W. Luo, Z. Li, Y. Liu, R.L. Withers, Nat. Mater. 9 (2010) 559–564.
[8] R.D. Smith, et al., Science 340 (2013) 60–63.
[9] L. Zhou, Y. Tan, J. Wang, W. Xu, Y. Yuan, W. Cai, S. Zhu, J. Zhu, Nat. Photonics 10 (2016) 393–398.
[10] L.J. France, et al., Appl. Catal. B Environ. 206 (2017) 203–215.
[11] K. Wang, J. Li, G. Zhang, ACS Appl. Mater. Interfaces 11 (2019) 27686–27696.
[12] Y. Zeng, K. Wang, J. Yao, H. Wang, Chem. Eng. Sci. 116 (2014) 704–709.
[13] N. Xu, X. Hu, W. Xu, X. Li, L. Zhou, S. Zhu, J. Zhu, Adv. Mater. 29 (2017).
[14] J. Wang, Y. Li, L. Deng, N. Wei, Y. Weng, S. Dong, D. Qi, J. Qiu, X. Chen, T. Wu, Adv. Mater. 29 (2017).
[15] Y. Wang, L. Zhang, P. Wang, ACS Sustain. Chem. Eng. 4 (2016) 1223–1230.
[16] J. Ren, S. Ouyang, H. Xu, X. Meng, T. Wang, D. Wang, J. Ye, Adv. Energy Mater. 7 (2017) 1601657.
[17] G. Chen, R. Gao, Y. Zhao, Z. Li, G.I.N. Waterhouse, R. Shi, J. Zhao, M. Zhang, L. Shang, G. Sheng, X. Zhang, X. Wen, L.Z. Wu, C.H. Tung, T. Zhang, Adv. Mater. 30 (2018).
[18] J. Bennie, T.W. Davies, J.P. Duffy, R. Inger, K.J. Gaston, Sci. Rep. 4 (2014) 3789.
[19] C. Xu, W. Huang, Z. Li, B. Deng, Y. Zhang, M. Ni, K. Cen, ACS Catal. 8 (2018) 6582–6593.
[20] P.G. Smirniotis, J. Catal. 334 (2016) 1–13.
[21] S.P. Luo, et al., Chem. Eng. J. 286 (2016) 291–299.
[22] M. Kang, E.D. Park, J.M. Kim, J.E. Yie, Appl. Catal. Gen. 327 (2007) 261–269.
[23] T. Zhang, W. Su, J. Li, Appl. Catal. B Environ. 176–177 (2015) 338–346.
[24] P. Sazama, R. Pilar, L. Mokrzycki, A. Vondrova, D. Kaucky, J. Plsek, S. Sklenak, P. Stastny, P. Klein, Appl. Catal. B Environ. 189 (2016) 65–74.
[25] H.-Y. Chen, Z. Wei, M. Kollar, F. Gao, Y. Wang, J. Szanyi, C.H.F. Peden, J. Catal. 329 (2015) 490–498.
[26] F. Gao, E.D. Walter, E.M. Karp, J. Luo, R.G. Tonkyn, J.H. Kwak, J. Szanyi, C.H. F. Peden, J. Catal. 300 (2013) 20–29.
[27] D.W. Fickel, et al., J. Phys. Chem. 2010 (2010) 1633–1640.
[28] J.H. Kwak, et al., J. Catal. 275 (2010) 187–190.
[29] D. Andreeva, Appl. Catal. Gen. 169 (1988) 9–14.
[30] N. Koukabi, E. Kolvari, A. Khazaei, M.A. Zolfigol, B. Shirmardi-Shaghasemi, H. R. Khavasi, Chem. Commun. 47 (2011) 9230.
[31] H. Tong, S. Ouyang, Y. Bi, N. Umezawa, M. Oshikiri, J. Ye, Adv. Mater. 24 (2012) 229–251.
[32] Y. Zeng, J. Yao, B.A. Horri, K. Wang, Y. Wu, D. Li, H. Wang, Energy Environ. Sci. 4 (2011) 4074.
[33] F. Liu, H. He, Catal. Today 153 (2010) 70–76.
[34] F. Liu, W. Shan, Z. Lian, J. Liu, H. He, Appl. Catal. B Environ. 230 (2018) 165–176.
[35] M. Milanese, G. Colangelo, A. Cretì, M. Lomascolo, F. Iacobazzi, A. de Risi, Sol. Energy Mater. Sol. Cells 147 (2016) 321–326.
[36] P. Hiralal, et al., Sol. Energy Mater. Sol. Cells 95 (2011) 1819–1825.
[37] L.J. Gao, et al., 2D Mater. 4 (2017), 025031.
[38] D. Li, R. Tan, J. Gao, B. Wei, Z. Fan, Q. Huang, K. He, Carbon 111 (2017) 428–438.
[39] F. Hu, S. Zhu, S. Chen, Y. Li, L. Ma, T. Wu, Y. Zhang, C. Wang, C. Liu, X. Yang, L. Song, X. Yang, Y. Xiong, Adv. Mater. 29 (2017).
[40] Y.G. Li, et al., Nat. Commun. 10 (2019) 2359.
[41] X. Miao, L. Zhang, L. Wu, Z. Hu, L. Shi, S. Zhou, Nat. Commun. 10 (2019) 3809.